J Braz. Soc. Mech. Sci. Eng. (2017) 39:1589–1596
DOI 10.1007/s40430-016-0687-3

TECHNICAL PAPER

Numerical study of non-Newtonian fluid flow over an exponentially stretching surface: an optimal HAM validation

Sajjad-ur-Rehman[1] · Rizwan-ul-Haq[2] · C. Lee[1] · S. Nadeem[3]

Received: 19 June 2015 / Accepted: 13 November 2016 / Published online: 24 November 2016

Abstract Present study is devoted to investigate the Casson fluid flow phenomena over an exponentially stretching surface at the heated wall. The stresses defined for Casson fluid model are reduced in the form of partial differential equations via boundary layer approximation and then converted into the system of nonlinear ODEs by means of similarity transformation. Present Casson fluid model is tackled via three different techniques: in which the numerical results are obtained through Runge–Kutta Felburge method and verified these results with the help of homotopy analysis method and modified technique known as optimal homotopy analysis method. Graphical comparisons and numerical tables are constructed to validate the results for three different techniques. The effects of each emerging parameters on velocity and temperature profiles are demonstrated through graphs. Moreover, skin friction and Nusselt number are also calculated and also provide the comparison between Newtonian fluid and non-Newtonian fluid. It is concluded that non-Newtonian fluid shows the higher skin friction coefficient as compared to Newtonian fluid, while the Nusselt number is more dominant for Newtonian case as compared to non-Newtonian case for different values of temperature exponent. Temperature exponent also play a significant role in heat transfer within the boundary layer domain.

Keywords 3-D flow · OHAM · Casson fluid model · Exponential stretching · Numerical solution

1 Introduction

In many engineering branches, such as chemical and material processing, most of the commonly working materials and liquids exhibit multifaceted rheological properties, whose viscosity and viscoelasticity can be reshape and continuously deformed by extracting some external conditions or forces, such as stress, strain, timescale and temperature. The flows of non-Newtonian fluids are considering great attention from researchers. These fluids can be used as coolant and heat exchangers and with this we can reduce pumping power. These fluids show shear-stress–strain relationship which is completely different from Newtonian model. In these fluids momentum conservation equation is modified. Time independent non-Newtonian fluids along with heat transfer are very much important and are widely used in food preserving and processing, power engineering and petroleum production. The fundamental governing equations for such complex fluids are highly nonlinear in the mathematical modeling as compared to Newtonian fluids. Most of the models have been discussed in literature for differential, integral and rate type classifications. Among different Non-Newtonian models Casson fluid model is also an important model which was first introduced by Casson in 1959. The Casson fluid model reveal yield stress if shear stresses is less than yield stress, somehow it pretend like a solid. If shear stress is higher than the yield stress then it comes into the motion. Studies related to this model can be found in [1–4].

Technical Editor: Cezar Negrao.

✉ Rizwan-ul-Haq
ideal_riz@hotmail.com

[1] Department of Computational Science and Engineering, Yonsei University, Seoul, Korea

[2] Department of Electrical Engineering, Bahria University Islamabad, Islamabad, Pakistan

[3] Department of Mathematics, Quaid-i-Azam University, Islamabad, Pakistan

In literature most of the studies are related to stretching surface, in which surface is stretched by keeping the origin fixed. Sakiadsi [5] was the first one who considered boundary layer flow over stretching surface. Later on Crane [6] investigated the flow over a stretching sheet. It was amended that velocity is directly proportional to the distance from the slit. Carragher [7] further extended the idea of Crane for heat transfer study to determine the Nusselt number for all possible date of Prandtl number. Heat distribution and fluid flow along a stretching surface with suction and blowing is presented by Gupta and Gupta [8]. Many other studies related to linear stretching surface are seen in [9–14].

All studies mentioned above are related to linear stretching, but not necessarily the stretching is linear, it can be considered as a nonlinear, power-law, and exponential form. In fact, most of the available physical situations in the literature have nonlinear stretching. Many researchers deal with this type of stretching by taking different assumptions such as Vajravelu [15] who discussed numerical solution for viscous flow over a nonlinear stretching heated surface. Similarly, Cortel [16] discussed the same problem with two different cases for nonlinear stretching sheet with assuming a constant surface temperature and second prescribed surface temperature. These types of stretching are discussed by many other authors by taking different fluid models and heat transfer phenomena see [17–20].

Some years ago, many researchers like Magyari and Keller [21], Elbashbeshy [22], Partha et al. [23], and Sanjayanand and Khan [24] dealt the heat and mass transfer phenomena along an exponentially stretching surface by taking several types of thermo-physical conditions. These types of stretching are much important in many industrial processes such as annealing and thinning copper wires, polymer processing, production of glass sheets, paper production. The most important factor that needs to be under consideration while production of any material is heat transfer rate when stretching velocity and temperature distributions are varies exponentially. Al-Odat et al. [25] discussed the magneto-hydrodynamic flow over an exponentially stretching sheet. Later, Sajid and Hayat [26] present analytical solution via homotopy analysis method (HAM) for exponentially stretching surface within the boundary layer domain. Afterwards several models are examined on the bases of exponentially stretching surface, particularly, for boundary layer phenomena under different aspects and by taking different types of fluid models along with heat transfer see [27–30].

Casson fluid is defined as a shear thinning liquid that leads to have infinite viscosity at zero shear stress, a yield stress is below that pretends no flow, and illustrate zero viscosity at infinite rate of shear. Due to such kind of behavior, studies conducted on Casson fluid model on various aspects are talked on the bases of stretching surface as a linear, nonlinear and exponential. Pramanik [31] studied the heat transfer for Casson fluid over exponential stretching surface along with thermal radiation. Nadeem et al. [32] considered MHD Casson fluid flow over exponential shrinking sheet. Some other features related to this model are discussed by many authors see [33–42].

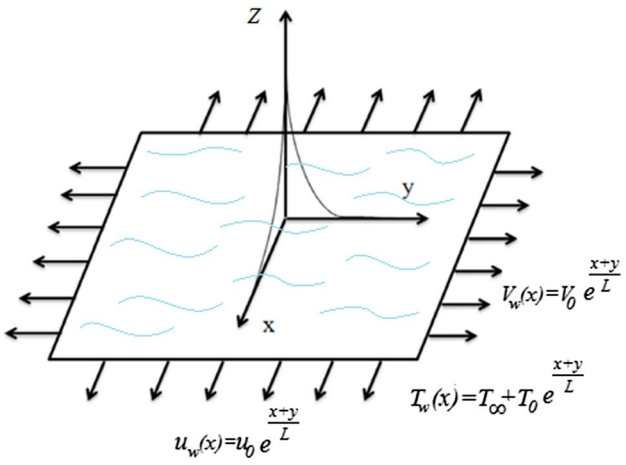

Fig. 1 Geometry of the problem

Main determination of this work is to discuss the idea for three dimensional Casson fluid flow over an exponentially stretching surface. We further consider the heated wall to illustrate the effects of Casson fluid. Moreover, present study is validated through different techniques (HAM, OHAM and Runge–Kutta Felburge method). In this study, we also present the comparison with existing literature. The heat transfer comparison for Newtonian and non-Newtonian fluid is studied. Graphical comparison is presented among above mentioned method. Comparisons for skin friction coefficient and Nusselt number with these three methods are plotted and conclusion has been drawn under the observations of whole analysis.

2 Mathematical modeling

Consider steady, incompressible flow of Casson fluid along an exponentially stretching surface in *xoy* plane and fluid is confine in $z > 0$. The component of exponential stretching velocity along x and y direction are U_w and V_w, respectively. Geometry of present model is configured in Fig. 1.

The rheological equation of state for an isotropic and incompressible flow of Casson fluid as reported by Nadeem et al. [32] is given by

$$\tau^{1/n} = \tau_0^{1/n} + \mu\dot{\gamma}^{1/n} \tag{1}$$

or

$$\tau_{ij} = \left[\mu_{\mathrm{B}} + \left(\frac{P_y}{\sqrt{2\pi}}\right)^{\frac{1}{n}}\right]^n 2e_{ij} \tag{2}$$

where $\mu, \mu_{\mathrm{B}}, P_y, \pi = e_{ij}e_{ij}$ are the dynamic viscosity, plastic dynamic viscosity, yield stress for Casson fluid and the product of the deformation rate, respectively. The governing equations of continuity, momentum and energy equation (absence of viscous dissipation) with constant physical properties for this model takes the following form,

$$\frac{\partial u}{\partial x} + \frac{\partial v}{\partial y} + \frac{\partial w}{\partial z} = 0, \tag{3}$$

$$u\frac{\partial u}{\partial x} + v\frac{\partial u}{\partial y} + w\frac{\partial u}{\partial z} = \upsilon\left(1 + \frac{1}{\beta}\right)\frac{\partial^2 u}{\partial z^2}, \tag{4}$$

$$u\frac{\partial v}{\partial x} + v\frac{\partial v}{\partial y} + w\frac{\partial v}{\partial z} = \upsilon\left(1 + \frac{1}{\beta}\right)\frac{\partial^2 v}{\partial z^2}, \tag{5}$$

$$u\frac{\partial T}{\partial x} + v\frac{\partial T}{\partial y} + w\frac{\partial T}{\partial z} = \frac{k}{\rho c_p}\frac{\partial^2 T}{\partial z^2}. \tag{6}$$

For this flow problem the boundary conditions are,

$$u = U_w, v = V_w, w = 0, T = T_w \quad at\ z = 0, \tag{7}$$

$$z \to \infty, u = 0, v = 0, T = T_\infty. \tag{8}$$

Here (u, v, w) are the velocity components, $\upsilon = {}^{\mu}/_{\rho}$ is kinematic viscosity and $\beta = \frac{\mu_B\sqrt{2\pi c}}{p_y}$ is the Casson fluid parameter. In addition, T is the temperature, k is the thermal conductivity, ρ is the density and c_p is the specific heat. U_w, V_w, and T_w denote the wall velocity and wall temperature, respectively. T_∞ is the ambient fluid temperature away from the wall.

The surface stretching velocities and the wall temperature for this study are assumed as describe by I. Notice that, following Chung Liu et al. [30] we use

$$U_w = U_0 e^{\frac{x+y}{L}}, V_w = V_0 e^{\frac{x+y}{L}}, T_w = T_\infty + T_0 e^{\frac{A(x+y)}{2L}}, \tag{9}$$

where U_0, V_0, and T_0 are constants. Here, L is the reference length. The following similarity transformations are obtained to switch the system of partial differential equations (PDEs) defined in Eqs. (4)–(6) into set of ODEs:

$$\left.\begin{aligned} &u = U_o e^{\frac{x+y}{L}} f'(\eta), v = U_o e^{\frac{x+y}{L}} g'(\eta), \\ &w = -\left(\frac{\upsilon U_o}{2L}\right)^{\frac{1}{2}} e^{\frac{x+y}{2L}}\left(f + \eta f' + g + \eta g'\right), \\ &T = T_\infty + T_o e^{\frac{A(x+y)}{2L}}\theta(\eta), \\ &\eta = -\left(\frac{\upsilon U_o}{2L}\right)^{\frac{1}{2}} e^{\frac{x+y}{2L}} z. \end{aligned}\right\} \tag{10}$$

Using similarity transformations, continuity equation is satisfied automatically, momentum and energy equations will take the following forms:

$$\left(1 + \frac{1}{\beta}\right)f''' = -(f+g)f'' + 2\left(f' + g'\right)f', \tag{11}$$

$$\left(1 + \frac{1}{\beta}\right)g''' = -(f+g)g'' + 2\left(f' + g'\right)g', \tag{12}$$

$$\theta'' = -\Pr(f+g)\theta' + \Pr A(f' + g')\theta. \tag{13}$$

In the presence of similarity transformations the boundary conditions become,

$$f(0) = g(0) = 0, \quad f'(0) = 1,\ g'(0) = \alpha,\ \theta(0) = 1, \tag{14}$$

$$f'(\infty) = g'(\infty) = 0, \quad \theta(\infty) = 0. \tag{15}$$

where the prime is the differentiation w.r.t η. Here, $\Pr = {}^{\mu c_p}/_{k}$ represents the Prandtl number. It should be noted that the parameter β appears in the reduced form of momentum, while the parameter $\alpha = {}^{V_0}/_{U_0}$(stretching ratio) appears in boundary conditions. While in the heat transfer problem contains two parameters: Prandtl number and temperature exponent A. Though system is three dimensional but we have some reduced cases according to stretching parameter α. Here it is noticed that when $\alpha = 0$, present phenomena will reduced to the case of two-dimensional flow. However, for $\alpha = 1$, it gives $f = g$ which shows that flow is axisymmetric. Moreover, for infinitely large value of β the system will be reduced for viscous flow.

The other quantities of physical interests are dimensionless skin friction and Nusselt number; these are given by:

$$C_{fx} = (Re_{\mathrm{x}})^{-1/2}\left(1 + \frac{1}{\beta}\right)f''(0), \tag{16}$$

$$C_{fy} = (Re_{\mathrm{x}})^{-1/2}\left(1 + \frac{1}{\beta}\right)g''(0), \tag{17}$$

$$Nu_x = (Re_{\mathrm{x}})^{\frac{1}{2}}\left(-\theta'(0)\right), \tag{18}$$

where Re is the local Reynold number.

3 Numerical methods

3.1 Homotopy analysis method

The dimensionless nonlinear ordinary differential equations (11)–(13) along with the boundary conditions (14) and (15) are solved first with homotopy analysis method which is proven as a powerful technique to solve

nonlinear problems. The basic idea of this method is based on the choice of operator and initial guesses. Based upon the boundary condition, the most suitable initial guess with respect to the given equation are:

$$f_0 = 1 - e^{-\eta}, g_0 = \alpha\left(1 - e^{-\eta}\right), \theta_0 = e^{-\eta}. \tag{19}$$

The linear operators are given by,

$$L_f = \frac{\mathrm{d}^3 f}{\mathrm{d}\eta^3} - \frac{\mathrm{d}f}{\mathrm{d}\eta}, L_g = \frac{\mathrm{d}^3 g}{\mathrm{d}\eta^3} - \frac{\mathrm{d}g}{\mathrm{d}n}, L_\theta = \frac{\mathrm{d}^2\theta}{\mathrm{d}\eta^2} - \theta. \tag{20}$$

From Eqs. (13)–(15), the nonlinear operators are expressed as

$$N_f[\hat{f}(\eta;q), \hat{g}(\eta;q)] = \left(1 + \frac{1}{\beta}\right)\frac{\partial^3 \hat{f}(\eta;q)}{\partial\eta^3} + (\hat{f}(\eta;q) + \hat{g}(\eta;q))\frac{\partial^2 \hat{f}(\eta;q)}{\partial\eta^2} - 2(\frac{\partial \hat{f}(\eta;q)}{\partial\eta} + \frac{\partial \hat{g}(\eta;q)}{\partial\eta})\frac{\partial \hat{f}(\eta;q)}{\partial\eta} \tag{21}$$

$$N_g[\hat{f}(\eta;q), \hat{g}(\eta;q)] = \left(1 + \frac{1}{\beta}\right)\frac{\partial^3 \hat{g}(\eta;q)}{\partial\eta^3} + (\hat{f}(\eta;q) + \hat{g}(\eta;q))\frac{\partial^2 \hat{g}(\eta;q)}{\partial\eta^2} - 2(\frac{\partial \hat{f}(\eta;q)}{\partial\eta} + \frac{\partial \hat{g}(\eta;q)}{\partial\eta})\frac{\partial \hat{g}(\eta;q)}{\partial\eta} \tag{22}$$

$$N_\theta[\hat{\theta}(\eta;q), \hat{f}(\eta;q), \hat{g}(\eta;q)] = \frac{\partial^3 \hat{\theta}(\eta;q)}{\partial\eta^3} + \mathrm{Pr}(\hat{f}(\eta;q) + \hat{g}(\eta;q))\frac{\partial \hat{\theta}(\eta;q)}{\partial\eta} - \mathrm{Pr}A(\frac{\partial \hat{f}(\eta;q)}{\partial\eta} + \frac{\partial \hat{g}(\eta;q)}{\partial\eta})\hat{\theta}(\eta;q). \tag{23}$$

Here $q \in [0,1]$ is embedding parameter which relates the deformation from zeroth deformation to mth order deformation.

The zeroth-order deformation equations and boundary conditions are:

$$(1-q)L_f[\hat{f}(\eta;q) - f_0(\eta)] = \hbar_f q N_f[\hat{f}(\eta;q), \hat{g}(\eta;q)], \tag{24}$$

$$(1-q)L_g[\hat{g}(\eta;q) - g_0(\eta)] = \hbar_g q N_g[\hat{f}(\eta;q), \hat{g}(\eta;q)], \tag{25}$$

$$(1-q)L_\theta[\hat{\theta}(\eta;q) - \theta_0(\eta)] = \hbar_\theta q N_\theta[\hat{\theta}(\eta;q), \hat{f}(\eta;q), \hat{g}(\eta;q)]. \tag{26}$$

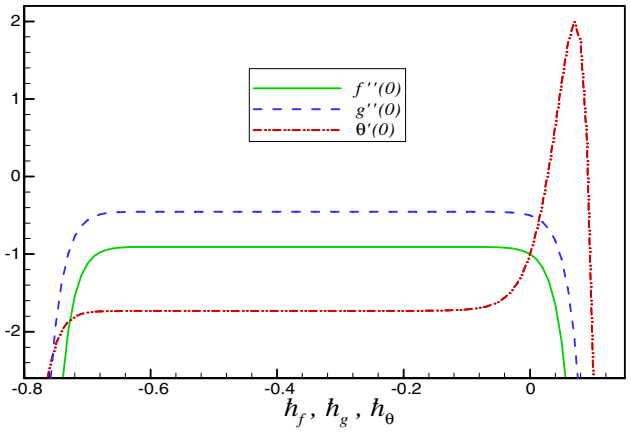

Fig. 2 Combine $\hbar$-curves at 20th order of approximation

The final solutions obtained by HAM are in the form of series defined as

$$\left.\begin{aligned} f(\eta) &= f_0(\eta) + \sum_{m=1}^{\infty} f_m(\eta), \\ g(\eta) &= g_0(\eta) + \sum_{m=1}^{\infty} g_m(\eta), \\ \theta(\eta) &= \theta_0(\eta) + \sum_{m=1}^{\infty} \theta_m(\eta). \end{aligned}\right\} \tag{27}$$

In this method, the convergence of the solution is strongly depends upon the convergence control parameters $\hbar_f$, $\hbar_g$ and $\hbar_\theta$. For suitable values of these parameters, we plot the so called $\hbar-$ curve at the 20th order approximation in Fig. 2. We observe that the suitable ranges for these parameters are $0 \le \hbar_f \le -0.70, 0 \le \hbar_g \le -0.75$, and $0.1 \le \hbar_\theta \le -0.75$.

3.2 Optimal homotopy analysis method

To obtain the optimized numerical value of emerging parameters, a moderate semi analytical technique (optimal HAM) is used by discretizing the squared residual error up to the finite mth iteration:

$$E_m^f \approx \frac{1}{N+1}\sum_{j=0}^{N}\left\{N_f\left[\sum_{i=0}^{m} f_i(\eta_j), \sum_{i=0}^{m} g_i(\eta_j)\right]\right\}^2, \tag{28}$$

$$E_m^g \approx \frac{1}{N+1}\sum_{j=0}^{N}\left\{N_f\left[\sum_{i=0}^{m} g_i(\eta_j), \sum_{i=0}^{m} f_i(\eta_j)\right]\right\}^2, \tag{29}$$

$$E_m^\theta \approx \frac{1}{N+1}\sum_{j=0}^{N}\left\{N_f\left[\sum_{i=0}^{m} \theta_i(\eta_j), \sum_{i=0}^{m} g_i(\eta_j), \sum_{i=0}^{m} f_i(\eta_j)\right]\right\}^2, \tag{30}$$

Table 1 Total average square residual errors for $\alpha = \frac{1}{2}, \beta = \frac{1}{2}, \mathrm{Pr} = 1, A = 2$

m	$\hbar_f$	$\hbar_g$	$\hbar_\theta$	E_m^T	CPU time (s)
02	−0.37953	−0.35668	−0.65871	1.7624×10^{-4}	5.91134
06	−0.39152	−0.36925	−0.57261	4.24968×10^{-7}	102.569
10	−0.46459	0.450223	−0.43630	2.57296×10^{-9}	1606.50

Table 2 Individual averaged square residual errors using optimal values at $m = 10$

m	E_m^f	E_m^g	E_m^θ	CPU time(s)
02	2.04248×10^{-5}	3.98235×10^{-5}	6.66396×10^{-4}	1.42008
06	9.62281×10^{-8}	2.24392×10^{-8}	1.29636×10^{-6}	10.9556
10	7.14953×10^{-10}	4.22651×10^{-10}	1.43536×10^{-9}	34.5765
20	2.99875×10^{-13}	4.54657×10^{-13}	1.18434×10^{-14}	209.286

where $\eta_j = j\Delta\eta$, $\Delta\eta = 0.5$ and $N = 20$. The total discrete square residual error is defined as

$$E_m^T = E_m^f + E_m^g + E_m^\theta, \tag{31}$$

$$\frac{\partial E_m^T}{\partial \hbar_f} = \frac{\partial E_m^T}{\partial \hbar_g} = \frac{\partial E_m^T}{\partial \hbar_\theta} = 0. \tag{32}$$

Tables 1 and 2 represent the optimized values "h" against the Eqs. (28)–(29). It can observed via Table 1, for each iteration total error against each "h" is attaining the zero total error. However, in Table 2, it is further analyzing that error of each function approaches zero for increasing values of m.

3.3 Numerical technique—Runge–Kutta Felburge method

Numerical approach has been proposed to validate the obtained optimized solutions through two different analytical techniques HAM and OHAM. For the system of coupled differential Eqs. (13)–(15) with boundary condition (16) and (17) are transformed into the initial value problem and then solved with the help of Runge–Kutta Felburge method. The size of each step is considered as $\Delta\eta = 0.01$ and the convergence criterion is fixed to 10^{-6}. The conditions defined in Eqs. (16) and (17) were replaced by $f(\eta_{\max}) = 1$ using a value similarity variable $\eta_{\max} = 12$. The choice of $\eta_{\max} = 12$ ensures that all numerical solutions approach the asymptotic values correctly.

4 Results and discussion

Before discussing the physical interpretation of the phenomena, it is important to validate present study with the existing literature. For this purpose, we construct a comparison in Table 3, in which numerical values have been computed for Nusselt number as $\beta \to \infty$. It is found that for Newtonian fluid our results exactly match with the study presented by Magyari and Keller [21] and Liu et al. [30]. In Table 4, we also present the comparison for skin friction coefficient for local Nusselt number with Liu et al. [30] for Newtonian fluid as $\beta \to \infty$.

The graphical comparison between the analytical methods and numerical method is plotted in Fig. 3. Notice that, the comparisons are done by calculating the skin friction coefficients along x and y-direction, and local Nusselt

Table 3 Comparison of the variation of local Nusselt number for Newtonian fluid as $\beta \to \infty$, at $\alpha = 0$

Pr ↓	A ↓	Magyari and Keller [21]	Liu et al. [30]	Present study		
				R. K. Felburge	HAM	OHAM
1	−1.5	0.37741	0.37741256	0.377412	0.37745	0.37758
	0	−0.549643	−0.54964375	−0.549646	−0.54969	−0.54961
	1	−0.954782	−0.95478270	−0.954786	−0.95471	−0.95470
	3	−1.560294	−1.56029540	−1.560295	−1.56026	−1.56024
5	−1.5	1.353240	1.35324050	1.3532405	1.35324	1.35328
	0	−1.521243	−1.52123900	−1.521240	−1.52123	−1.52126
	1	−2.500135	−2.50013157	−2.500135	−2.50017	−2.50049
	3	−3.886555	−3.88655510	−3.886555	−3.88659	−3.88655
10	−1.5	2.200000	2.20002816	2.2000282	2.20004	2.20002
	0	−2.257429	−2.25742372	−2.257424	−2.25747	−2.25747
	1	−3.660379	−3.66037218	−3.660372	−3.66038	−3.66035
	3	−5.635369	−5.62819631	−5.628196	−5.62817	−5.62815

Table 4 Comparison of local Nusselt number for Newtonian case as $\beta \to \infty$

α	Pr	$A=-2$		$A=0$		$A=2$	
		Liu et al. [30]	Present study	Liu et al. [30]	Present study	Liu et al. [30]	Present study
0.0	0.7	0.6236183	0.62362	−0.4258380	−0.42584	−1.6416592	−1.64166
	7.0	5.9409444	5.94093	−1.8466056	−1.84661	−5.8978037	−5.89780
0.5	0.7	0.7637845	0.76377	−0.5215410	−0.52154	−2.0106136	−2.01061
	7.0	7.2761412	7.27614	−2.2616208	−2.26162	−7.2233049	−7.22331
1.0	0.7	0.8819431	0.88194	−0.6022235	−0.60222	−2.3216566	−2.32164
	7.0	8.4017642	8.40175	−2.6114948	−2.61150	−8.3407540	−8.34075

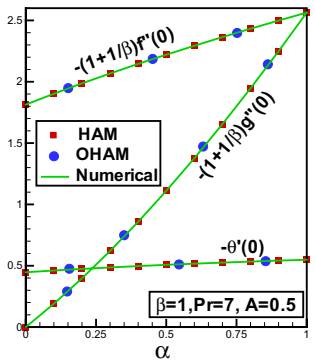

Fig. 3 Graphical comparison among three different techniques (numerical, HAM and OHAM) for skin friction confident and local Nusselt number

number against stretching ratio parameter α while rests of the emerging parameters are kept fixed. Excellent agreement between the three methods is obtained.

To discuss the fluid flow behavior and heat transfer near the wall, we have plotted the skin friction coefficient along *x*, *y*-direction and local Nusselt number in Fig. 4. Comparison between the Newtonian fluid ($\beta \to \infty$) and non-Newtonian fluid ($\beta = 0.5, 1$) are plotted. No doubt, non-Newtonian fluid has higher friction with the wall as compared to Newtonian fluid; these comparable results can be observed through Fig. 4a. Moreover, when $\alpha = 0$, there is no contribution in the variation of skin friction along y-direction. At $\alpha = 0.5$, variation in skin friction along x-direction provides a maximum contribution as compared to variation of skin friction along y-direction. Finally, at $\alpha = 1$ for axisymmetric case, variation in skin friction along *x* and *y* direction are similar.

Effect of both stretching ratio parameter and Casson fluid parameter for local Nusselt number are plotted in Fig. 4a. It can be observed that with the increase in the stretching ratio parameter, the local Nusselt number increases. Moreover, dominant difference between heat transfer at the wall for both Newtonian and non-Newtonian can be observed through Fig. 4b. Simultaneous effects of Prandtl number and temperature exponent $A = -0.5, 0$ and 2 for local Nusselt number are plotted in Fig. 4c. We observe a maximum influence to enhance the heat transfer near the wall with the increase of Prandtl number is obtained at $A = -0.5$. Moreover, it is found that the case of two-dimensional Newtonian fluid has less heat transfer

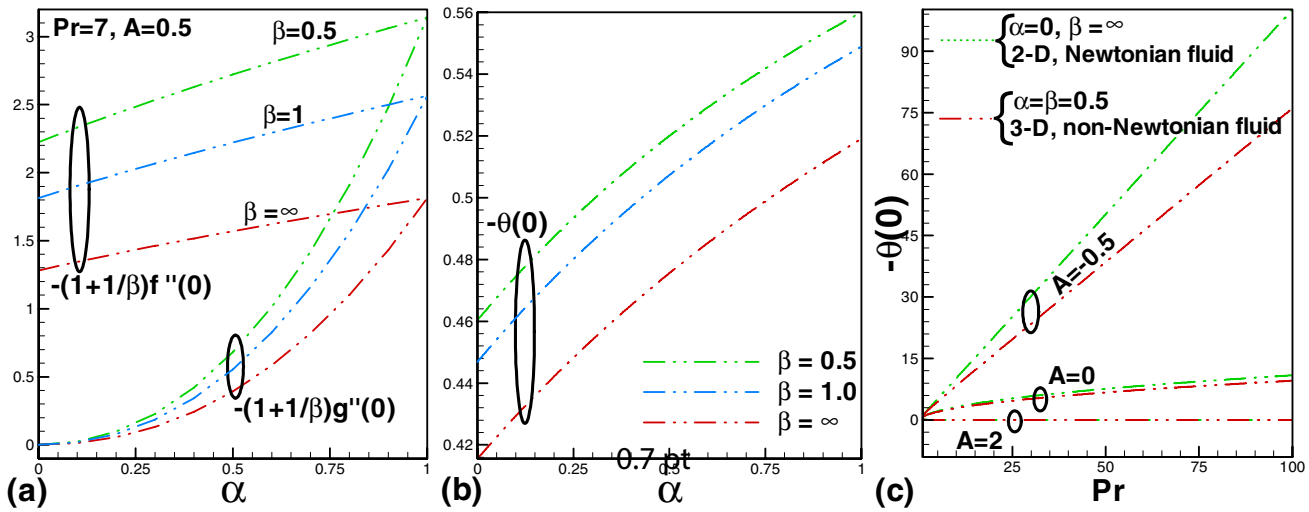

Fig. 4 Distribution of skin friction and local Nusselt number for several values of physical parameters

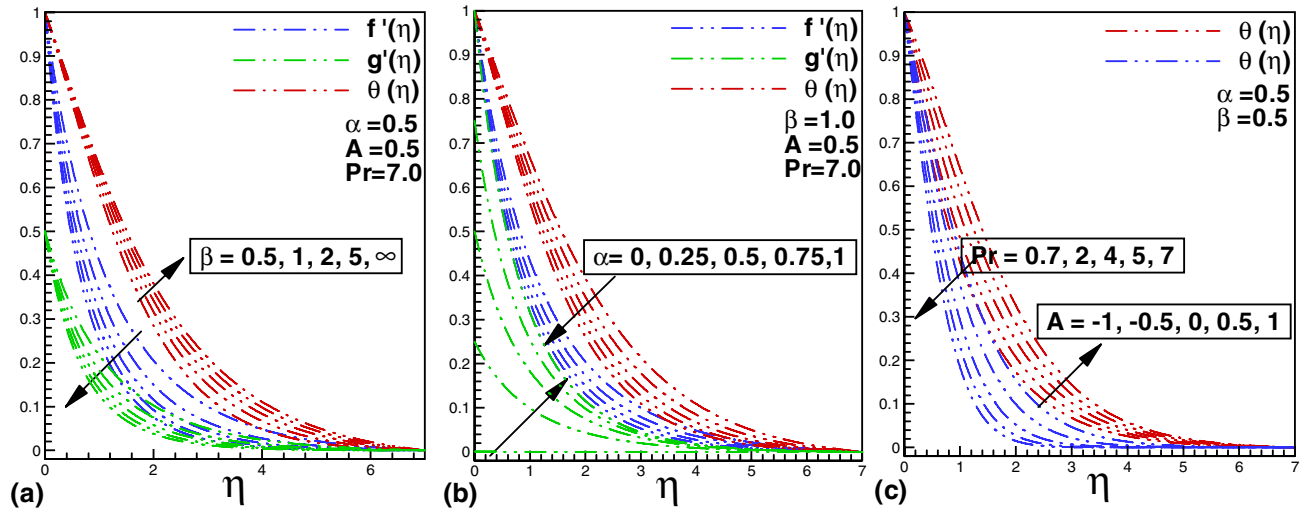

Fig. 5 Velocity and temperature distributions for various values of **a** β, **b** α, **c** Pr and A

in the vicinity of the boundary as compared to the three-dimensional non-Newtonian fluid. Similar effects can be seen for $A = 0$, but both two-dimensional Newtonian fluid and three-dimensional non-Newtonian fluid have same heat transfer rate with the wall for $A = 2$.

In Fig. 5, results for velocity and temperature profiles within the boundary layer are plotted against the emerging parameters. Variation of velocity along x and y directions with Casson fluid parameter β are plotted in Fig. 5a. We can observe that with the increase of non-Newtonian fluid parameter gives low velocity profile along both directions, while increasing effects can be observed in the case of temperature profile with the increase in the value of Casson fluid parameter. Figure 5b, shows the variation of velocities along both (x and y directions) and temperature distribution with increasing values of stretching ratio parameter α. It is further observed that velocity along x-direction and temperature profile ar decreasing as α increases. While increase in the variation of velocity along y-direction for various values of α. Figure 5c shows the effect of Prandtl number and temperature exponent on temperature profile. Both parameters give opposite effects on temperature profile, however, temperature exponent have dominant effects on temperature profile.

5 Concluding remarks

In the whole analysis, we construct a complete physical model of a stretching sheet along the x and y-directions while fluid is containing along the z-direction. So the main key findings are summarized as follows:

1. Non-Newtonian fluid shows higher skin friction coefficient as compared to Newtonian fluid. Moreover, the Nusselt number is more dominant for Newtonian fluid as compared to non-Newtonian fluids at different values of temperature exponents.
2. Velocity profile for both directions is decreasing with the increase in Casson fluid parameter, but temperature profile shows increasing behavior.
3. When stretching ratio is increased, both the velocity profile along x-direction and temperature profile are decreased. However, opposite behavior is observed for velocity profile along y-direction when stretching ratio is increased.
4. Boundary layer is inversely proportional to Prandtl number. Therefore, as Prandtl number increases, the boundary layer thickness decreases which causes a temperature decrease.
5. Temperature exponent also plays vital role in heat transfer as seen. More precisely, as the temperature exponent increases then temperature inside the fluid increases.
6. The mathematical methods used to solve the present physical model shows excellent agreement with previous available studies, which confirms the validity of the present physical results.

Acknowledgements This research was supported by a National Research Foundation of Korea (NRF) Grant funded by Korean Government (MSIP) (20090093134, 2014R1A2A2A01006544).

References

1. Fung YC (1984) Biodynamics: circulation. Springer-Verlag, New York
2. Dash RK, Metha KN, Jayaraman G (1996) Casson fluid flow in pipe filled with a homogenous porous Medium. Int J Eng Sci 34(10):1145–1156

3. Eldabe NTM, Salwa MGE (1995) Heat transfer of MHD non-Newtonian Casson fluid flow between two rotating cylinders. J Phys Soc Japan 64:41–64
4. Boyd J, Buick JM, Green S (2007) Analysis of the Casson and Carreau-Yasuda non-Newtonian blood models in steady and oscillatory flow using the lattice Boltzmann method. Phys Fluids 19:93–103
5. Sakiadis BC (1961) Boundary layer behavior on continuous solid surface: I Boundary layer equations for two dimensional and axisymmetric flow. AIChE J 7(1):26–28
6. Crane LJ (1970) Flow past a stretching plate. ZAMP 21:645
7. Carragher P (1978) Boundary layer flow and heat transfer the stretching plate. Ph.D.Thesis, University of Dublin, Chapter, 4: 41
8. Gupta PS, Gupta AS (1977) Heat and mass transfer on a stretching sheet with suction or blowing. Can J Chem Eng 55:744–746
9. Ellahi R, Shivanian E, Abbasbandy S, Hayat T (2016) Numerical study of magnetohydrodynamics generalized Couette flow of Eyring-Powell fluid with heat transfer and slip condition. Int J Num Methods Heat Fluid Flow 26(5):1433–1445
10. Khan A, Muhammad S, Ellahi R, Zaigham Q, Zia M (2016) Bionic study of variable viscosity on MHD peristaltic flow of Pseudoplastic fluid in an asymmetric channel. J Mag 21(2):273–228
11. Ellahi R (2014) The thermodynamics, stability, applications and techniques of differential type: a review. Rev Theor Sci 2:116–123
12. Ellahi R (2013) The effects of MHD and temperature dependent viscosity on the flow of non-Newtonian nanofluid in a pipe: analytical solutions. Appl Math Model 37(3):1451–1457
13. Ellahi R, Aziz S, Zeeshan A (2013) Non-Newtonian fluid flow through a porous medium between two coaxial cylinders with heat transfer and variable viscosity. J Porous Media 16(3):205–216
14. Rahman SU, Ellahi R, Nadeem S, Zaigham Zia QM (2016) Simultaneous effects of nanoparticles and slip on Jeffrey fluid through tapered artery with mild stenosis. J Mol Liq 218:484–493
15. Vajravelu K (2001) Viscous flow over nonlinear stretching sheet. Appl Math Comp 124:281–288
16. Cortell R (2007) Viscous flow and heat transfer over nonlinearly stretching sheet. Appl Math Comp 184:864–873
17. Ali Mohamed E (1995) On thermal boundary layer on a power-law stretched surface with suction or injection. Int J Heat Fluid Flow 16:280–290
18. Chamkha Ali J (1997) Similarity solution for thermal boundary layer on a stretched surface of non-Newtonian fluid. Int Commun Heat Mass Transf 24(5):643–652
19. Robert A. Van Gorder, K. Vajravelu, F. Talay Akyildiz (2011) Existence and uniqueness results for a nonlinear differential equation arising in viscous flow over nonlinear stretching sheet. Appl Math Lett 24: 238–242
20. Parsad KV, Vajravelu K, Datti PS (2010) Mixed convective heat transfer over a non-linear stretching surface with variable fluid properties. Int J Non-Linear Mech. 45(3):320–330
21. Magyari E, Keller B (1999) Heat and mass transfer in the boundary layer over an exponentially stretching continuous surface. J Phys D Appl Phys 32:577–585
22. Elbashbeshy EMA (2001) Heat transfer over an exponentially stretching continuous surface with suction. Arch Mech 53:643–651
23. Partha MK, Murthy PVSN, Rajasehkar GP (2005) Effect of viscous dissipation on the mixed convection heat transfer from an exponentially stretching surface. Heat Mass Transf. 41:360–366
24. Sanjayanand E, Khan SK (2006) Boundary layer viscoelastic fluid flow over an exponentially stretching sheet. Int J Appl Mech Eng 11:321–335
25. Al-Odat MQ, Damesh RA, Al-Azab TA (2006) Thermal boundary layer on an exponentially stretching continuous surface in the presence of magnetic field effect. Int J Appl Mech 11(2):289–299
26. Sajid M, Hayyat T (2008) Influence of thermal radiation on the boundary layer flow due to an exponentially stretching sheet. Int Commun Heat Mass Transf. 35:347–356
27. El-Aziz MA (2009) Viscous dissipation effect on mixed convection flow of a micro polar fluid over an exponentially stretching sheet. Can J Phys 87:359–368
28. Nadeem S, Zaheer S, Fang T (2011) Effects of thermal radiation on the boundary layer flow of a Jeffrey fluid over an exponentially stretching surface. Num Algorithms 57:187–205
29. Ishak A (2011) MHD boundary layer flow due to an exponentially stretching sheet with radiation effect. Sians Malays 40:391–405
30. Liu IC, Wang HH, Peng YF (2013) Flow and heat transfer for three dimensional flow over an exponentially stretching surface. Chem Eng Commun 200:253–268
31. Pramanik S (2013) Casson fluid flow and heat transfer past an exponentially porous stretching surface in presence of thermal radiation. A. S. Eng J. 5:205–212
32. Nadeem S, Haq Rizwan Ul, Lee C (2012) MHD flow of Casson fluid over an exponentially shrinking sheet. Scientia Iranica. 19(6):1550–1553
33. Shahzad A, Ali R, Khan M (2012) On the exact solution for axisymmetric flow and heat transfer over a nonlinear radially stretching sheet. Chin Phys Lett 29(8):084705
34. Shahzad A, Ali R (2012) Approximate analytic solution for magneto-hydrodynamic flow of a non-Newtonian fluid over a vertical stretching sheet. Can J Appl Sci 2:202–215
35. Shahzad A, Ali R (2013) MHD flow of a non-Newtonian Power law fluid over a vertical stretching sheet with the convective boundary condition. Walailak J Sci Technol 10(1):43–56
36. Ahmed J, Shahzad A, Khan M (2015) A note on convective heat transfer of an MHD Jeffrey fluid over a stretching sheet. AIP Adv 5(11):117117
37. Ramzan M, Bilal M, Chung Jae Dong (2016) Effects of MHD homogeneous-heterogeneous reactions on third grade fluid flow with Cattaneo-Christov heat flux. J Mol Liq 223:1284–1290
38. Nadeem S, Haq Rizwan Ul, Akbar Noreen Sher, Khan ZH (2013) MHD three-dimensional Casson fluid flow past a porous linearly stretching sheet. Alex Eng J 52(4):577–582
39. Ramzan M, Bilal M (2015) Time dependent MHD nano-second grade fluid flow induced by permeable vertical sheet with mixed convection and thermal radiation. PLoS One 10(5):e0124929
40. Ramzan M, Bilal M (2016) Three-dimensional flow of an elastico-viscous nanofluid with chemical reaction and magnetic field effects. J Mol Liq 215:212–220
41. Al-Mdallal QM, Syam MI, Ariel PD (2011) Extended homotopy perturbation method and the axisymmetric flow past a porous stretching sheet. Int J Num Methods Fluids 69(5):909–925
42. Al-Mdallal QM, Syam MI, Ariel PD (2013) The extended homotopy perturbation method and boundary layer flow due to condensation and natural convection on a porous vertical plate. Int J Comput Math 88(16):3535–3552